



# Kent Academic Repository

Pickup, David M., Speight, Richard J., Knowles, Jonathan C., Smith, Mark E. and Newport, Robert J. (2008) *Sol-gel synthesis and structural characterisation of binary TiO<sub>2</sub>-P<sub>2</sub>O<sub>5</sub> glasses*. *Materials Research Bulletin*, 43 (2). pp. 333-342. ISSN 0025-5408.

## Downloaded from

<https://kar.kent.ac.uk/15960/> The University of Kent's Academic Repository KAR

## The version of record is available from

<https://doi.org/10.1016/j.materresbull.2007.03.005>

## This document version

UNSPECIFIED

## DOI for this version

## Licence for this version

UNSPECIFIED

## Additional information

## Versions of research works

### Versions of Record

If this version is the version of record, it is the same as the published version available on the publisher's web site. Cite as the published version.

### Author Accepted Manuscripts

If this document is identified as the Author Accepted Manuscript it is the version after peer review but before type setting, copy editing or publisher branding. Cite as Surname, Initial. (Year) 'Title of article'. To be published in *Title of Journal*, Volume and issue numbers [peer-reviewed accepted version]. Available at: DOI or URL (Accessed: date).

## Enquiries

If you have questions about this document contact [ResearchSupport@kent.ac.uk](mailto:ResearchSupport@kent.ac.uk). Please include the URL of the record in KAR. If you believe that your, or a third party's rights have been compromised through this document please see our [Take Down policy](https://www.kent.ac.uk/guides/kar-the-kent-academic-repository#policies) (available from <https://www.kent.ac.uk/guides/kar-the-kent-academic-repository#policies>).

## Sol–gel synthesis and structural characterisation of binary $\text{TiO}_2\text{--P}_2\text{O}_5$ glasses

David M. Pickup<sup>a,\*</sup>, Richard J. Speight<sup>b</sup>, Jonathan C. Knowles<sup>c</sup>,  
Mark E. Smith<sup>b</sup>, Robert J. Newport<sup>a</sup>

<sup>a</sup>*School of Physical Sciences, University of Kent, Canterbury CT2 7NH, UK*

<sup>b</sup>*Department of Physics, University of Warwick, Coventry CV4 7AL, UK*

<sup>c</sup>*Division of Biomaterials and Tissue Engineering, UCL Eastman Dental Institute, 256 Gray's Inn Road, London WC1X 8LD, UK*

Received 25 September 2006; received in revised form 27 February 2007; accepted 1 March 2007

Available online 6 March 2007

### Abstract

An improved method for the sol–gel synthesis of binary  $(\text{TiO}_2)_{0.5}(\text{P}_2\text{O}_5)_{0.5}$  glasses has been developed. Elemental analysis of the products showed that the loss of phosphorous upon drying and heat treatment is low. The structure of the heat-treated glasses was studied using neutron diffraction and high-energy X-ray diffraction, analysis of which revealed a structure consisting of  $\text{PO}_4$  tetrahedra and  $\text{TiO}_6$  octahedra sharing corners in a three-dimensional amorphous network. The Reverse Monte Carlo method was used to produce a structural model which illustrated that the structure of the glass is, at the near-neighbour level, closely analogous to the superstructure of crystalline  $\text{TiP}_2\text{O}_7$ . No significant atomic-scale structural differences were observed between glasses prepared by acid- or base-catalysed sol–gel reactions.

© 2007 Elsevier Ltd. All rights reserved.

*Keywords:* A. Amorphous materials; B. Sol–gel chemistry; C. Neutron scattering; C. X-ray diffraction

### 1. Introduction

The sol–gel method can be used to prepare  $\text{TiO}_2\text{--P}_2\text{O}_5$  glasses over a wide-range of compositions containing 30–90 mol% titania [1,2]. Such glasses have a variety of interesting properties and potential applications. Glasses containing large amounts of  $\text{TiO}_2$  are expected to have high linear and non-linear refractive indices. Such glasses are widely investigated for potential future photonics application because of their fast response time, high transparency, isotropy and good compatibility with waveguide and fibre fabrication [1]. Sol–gel glasses with a higher  $\text{P}_2\text{O}_5$  content (~70 mol%) can be prepared as proton-conducting glassy films. These films are chemically highly durable and very sensitive to relative humidity and thus have potential for use in humidity sensors. Additions of  $\text{CaO}$  and  $\text{Na}_2\text{O}$  to the  $\text{TiO}_2\text{--P}_2\text{O}_5$  system produce materials with properties suitable for biomedical applications [3]. Such materials can be prepared to be bioresorbable, with the release of  $\text{Ca}^{2+}$  ions stimulating cell proliferation.

Preparing  $\text{TiO}_2\text{--P}_2\text{O}_5$  glasses by a sol–gel route has some significant advantages over melt-quenching techniques. The preparation of high  $\text{TiO}_2$ -content glasses for non-linear optical applications by melt-quenching suffers from two severe limitations. Firstly, the upper limit of  $\text{TiO}_2$  content for glass formation by melt-quenching is 74 mol%, and

\* Corresponding author. Tel.: +44 1227823043; fax: +44 1227827558.

E-mail address: [dmp@kent.ac.uk](mailto:dmp@kent.ac.uk) (D.M. Pickup).

secondly, such glasses are deeply coloured purple due to the presence of a significant amount of  $Ti^{3+}$  rendering them unsuitable for optical applications. These two problems are negated by the use of sol–gel chemistry which allows the preparation of highly transparent monoliths containing up to 90 mol%  $TiO_2$ . There are two further key benefits of the sol–gel process: glassy films can be prepared, and the processing can be modified to produce porous materials. The advantage of introducing porosity is relevant to the potential applications of these materials in the fields of sensors, ion-exchangers and biomaterials.

We have recently developed a new sol–gel route to  $TiO_2$ – $P_2O_5$  glasses based on the reaction of titanium isopropoxide with *n*-butyl phosphate. We have characterised these glasses and studied their structure using a combination of neutron diffraction (ND) and high-energy X-ray diffraction (HEXRD). The Reverse Monte Carlo modelling method has been applied to produce a model of the structure that is consistent with the experimental data.

## 2. Experimental methods

### 2.1. Sample preparation

The following reagents were purchased commercially and used without further purification: titanium isopropoxide ( $Ti(OPr^i)_4$ , Aldrich, >95%), 1:1 molar mixture of monobutyl and dibutyl *n*-butyl phosphate ( $OP(OH)_2(OBu^n)$  and  $OP(OH)(OBu^n)_2$ , Alfa Aesar, ~98%), 2-methoxyethanol (MeO–EtOH, Aldrich, 99.8%), isopropanol ( $Pr^iOH$ , Aldrich, 99.5%), *n*-butanol ( $Bu^nOH$ , Aldrich, 99.8%), hydrochloric acid (Fisher, 37 wt%) and ammonia solution (Aldrich, 28 wt% in water).

All reactions were carried out under dry conditions in a sealed vessel with magnetic stirring. The acid-catalysed reaction entailed first diluting the  $Ti(OPr^i)_4$  in 2-methoxyethanol at a molar ratio of 1:9.5. After allowing this mixture to cool (approximately 15 min), *n*-butyl phosphate was added using a syringe pump at a rate of 20 ml/h such that the molar ratio of  $Ti(OPr^i)_4$  to *n*-butyl phosphate was 1:2. The titanium and phosphorus precursors were allowed to react for 1 h before cooling in an ice bath and adding a solution containing  $H_2O$  and the HCl catalyst in a solvent at a rate of 300 ml/h using a syringe pump. The  $H_2O$ /HCl/solvent mixture consisted of  $H_2O$ :HCl: $Pr^iOH$ : $Bu^nOH$  in the molar ratio 2:0.05:2.9:2.4 relative to the amount of  $Ti(OPr^i)_4$  used. The resultant clear sol was poured into a polypropylene container and allowed to gel which took around 5 min.

The base-catalysed synthesis was similar to that described above. Firstly, the *n*-butyl phosphate was diluted in *n*-butanol (molar ratio 1:4). Secondly, the reaction vessel was placed in an ice bath and the  $Ti(OPr^i)_4$  added using a syringe pump at a rate of 20 ml/h (molar ratio of Ti:P of 1:2). After 1 h, a solution of  $NH_3$  catalyst, water and solvent was added at a rate of 100 ml/h. The composition of this solution was the same as for the acid-catalysed reaction. The clear sol was removed from the ice bath and poured into a polypropylene container. Gellation took approximately 2 min and the gel turned opaque after 30 min.

All samples were aged at room temperature for 7 days in sealed containers before drying at 60 °C. The dried gels were heated to 500 °C to remove solvent, water and organic molecules. Characterisation necessary for analysis of the neutron and X-ray diffraction data was performed: elemental analysis (ICP-AES and gravimetric) was carried out by a commercial company (Medac Ltd.) and macroscopic densities were determined by helium pycnometry using a Quantachrome Multipycnometer. The results of this characterisation are presented in Table 1.

### 2.2. Neutron and X-ray diffraction measurements

The neutron diffraction data presented here were collected on the GEM diffractometer on the ISIS spallation neutron source at the Rutherford Appleton Laboratory, UK. The finely powdered samples were held in 8 mm diameter

Table 1  
Sample characterisation of heat-treated  $TiO_2$ – $P_2O_5$  sol–gel glasses

Sample name	Catalyst	Nominal composition	Measured composition (at%)					Density (g cm <sup>-3</sup> )
			P	Ti	O	C	H	
P50T50A	Acid	$(TiO_2)_{0.5}(P_2O_5)_{0.5}$	16.88	9.90	61.99	6.73	4.50	2.36(5)
P50T50B	Base	$(TiO_2)_{0.5}(P_2O_5)_{0.5}$	16.56	9.19	59.78	9.76	4.70	2.39(5)

vanadium foil cans, which have a very low cross-section for the coherent scattering of neutrons, and time-of-flight data collected over a wide-range of  $Q$  (up to  $50 \text{ \AA}^{-1}$ , where  $Q = 4\pi \sin \theta/\lambda$  and  $2\theta$  is the scattering angle). The program GUDRUN was used to reduce and correct the data [4]. The samples studied contained a significant amount of hydrogen which gave rise to a high level of incoherent scattering. The data were fitted with Chebyshev polynomials to correct for this in an empirical fashion.

The high-energy X-ray diffraction data were collected on Station 9.1 at the synchrotron radiation source (SRS), Daresbury Laboratory, UK. The finely powdered samples were enclosed inside a 0.5 mm thick circular metal annulus by kapton windows and mounted onto a flat-plate instrumental set-up. The wavelength was set at  $\lambda = 0.4858 \text{ \AA}$ , and calibrated using the K-edge of an Ag foil; this value was low enough to provide data to a high value of momentum transfer ( $Q_{\text{max}} \sim 23 \text{ \AA}^{-1}$ ). The data were corrected using a suite of programs written in-house, which were themselves based upon the method of Warren [5].

The initial stage of analysis of diffraction data from an amorphous material involves the removal of background scattering, normalisation, correction for absorption, inelastic and multiple scattering and subtraction of the self-scattering term [4,6]. In the case of the HEXRD data, no correction was made to account for multiple scattering since it may be shown to be negligible for an optically thin, low atomic number sample, such as those studied here. The resultant scattered intensity,  $i(Q)$ , can reveal structural information by Fourier transformation to obtain the pair distribution function:

$$T(r) = T^0(r) + \int_0^\infty Q i(Q) M(Q) \sin(Qr) dQ \quad (1)$$

where  $T^0(r) = 2\pi^2 r \rho_0$  ( $r$  is the atomic separation between atoms and  $\rho_0$  the macroscopic number density) and  $M(Q)$  is a window function necessitated by the finite maximum experimentally attainable value of  $Q$ .

Structural information can be obtained from the diffraction data by simulating the  $Q$ -space data and converting the results to  $r$ -space by Fourier transformation to allow comparison with the experimentally determined correlation function [7]. The  $Q$ -space simulation is generated using the following equation:

$$p(Q)_{ij} = \frac{N_{ij} w_{ij}}{c_j} \frac{\sin QR_{ij}}{QR_{ij}} \exp\left[\frac{-Q^2 \sigma_{ij}^2}{2}\right] \quad (2)$$

where  $p(Q)_{ij}$  is the pair function in reciprocal space,  $N_{ij}$ ,  $R_{ij}$  and  $\sigma_{ij}$  are the coordination number, atomic separation and disorder parameter, respectively, of atom  $i$  with respect to  $j$ ,  $c_j$  the concentration of atom  $j$  and  $w_{ij}$  is the weighting factor. In the case of the ND, the weighting factors are

$$w_{ij} = \frac{2c_i c_j b_i b_j}{\bar{b}^2} \quad \text{if } i \neq j \quad (3)$$

or,

$$w_{ij} = \frac{c_i^2 b_i^2}{\bar{b}^2} \quad \text{if } i = j \quad (4)$$

where  $b$  represents the coherent scattering length. In the case of the HEXRD, the weighting factors are of the same form, but with the  $Q$ -independent neutron scattering lengths replaced by the  $Q$ -dependant X-ray form factors,  $f(Q)$ .

In this work, both the ND and HEXRD data were simulated *simultaneously* to produce one set of fitted structural parameters per sample. In this way, the position and width of each of the principal pair correlation peaks may be fitted via the simulated  $i(Q)$ . The approach is usually limited, at best, to the nearest and next-nearest neighbours because of the difficulty in coping with overlapping correlations; the availability of data from both ND and HEXRD does, however, offer two significant advantages. Firstly, it allows for more robust assignment of the features in the pair distribution function because of the difference in the weighting factors associated with the two techniques. This is especially important for  $r$ -space features where the problem of overlapping correlations makes peak assignment particularly difficult. Thus, to constrain the simulated intensities to be consistent with the two distinct experimental  $i(Q)$  profiles means that the problem of ill-determined peak assignments is greatly reduced. The second advantage of fitting both datasets together is that it gives a more reliable estimate of the errors introduced during the data reduction process. Assuming that the model is correct, discrepancies between the fits to the two datasets are most likely to be due

to errors in the corrections to the experimental data. These errors can be used to produce tolerances that better reflect the true uncertainties in the structural parameters derived from the fitting/modelling process.

### 2.3. Reverse Monte Carlo modelling

In order to produce a heuristic three-dimensional model of the glass structure that is consistent with the experimental data, the Reverse Monte Carlo (RMC) method was employed [8]. RMC modelling involves minimizing the difference between an interference function calculated from a model configuration of atomic positions (i.e. a computer generated “box of atoms” established using periodic boundary conditions, and experimental values for the density, composition and hard sphere radii) and an experimentally measured interference function. The minimisation is achieved by moving the atoms in the configuration at random and accepting or rejecting the moves on the basis of how they affect the correlation between the calculated and experimental data. The resulting configuration is a three-dimensional structure consistent with the experimental data within experimental error. The model constructed here was derived from a box filled according to the superstructure of crystalline  $\text{TiP}_2\text{O}_7$  [9,10] and consisted of 1080 atoms in a cubic box with a side length of 23.534 Å giving a density of 0.0829 atoms Å<sup>-3</sup> (i.e. the density of crystalline  $\text{TiP}_2\text{O}_7$ ). The atom types were 217 P, 107 Ti and 756 O to give a composition very close to that of  $\text{TiP}_2\text{O}_7$ . This starting configuration was modified using the RMC algorithm to produce a model consistent with the HEXRD data. The RMC method was only applied to the HEXRD data because of the presence of residual C and H in the samples (see Table 1), the scattering from which has a more significant contribution to the ND data; the presence of C and H at low levels can essentially be ignored in the case of HEXRD, making the RMC model simpler. Furthermore, it is unlikely that by including C and H in the model, any useful structural information concerning the structural environment of these elements could be obtained since the carbon, and at least some of the hydrogen, are present in organic fragments residual from the sol–gel process and are therefore not part of the glass structure. To ensure that the model of the glass was sufficiently independent of the crystalline starting configuration, the RMC algorithm was run until  $\sim 1.5 \times 10^6$  moves had been accepted; this equates to  $\sim 1500$  moves per atom, with the size of each move ranging from 0.02 to 0.1 Å.

## 3. Results and discussion

### 3.1. Sample preparation

The results of the elemental analysis in Table 1 show that the loss of phosphorus occurring during the sol–gel process presented here is relatively low. The calculated loss of phosphorus for the two samples analysed is 15% for the acid-catalysed sample and 10% for the base-catalysed sample. This compares favourably with the  $\sim 75\%$  phosphorus loss experienced during some of our earlier attempts to prepare  $(\text{TiO}_2)_{0.5}(\text{P}_2\text{O}_5)_{0.5}$  sol–gels using triethyl phosphate  $(\text{OP}(\text{OEt})_3)$  as the phosphorus precursor. Such an excessive loss was attributed to the slow hydrolysis rate of  $\text{OP}(\text{OEt})_3$  which prevents the bulk of the phosphorus taking part in the sol–gel reaction to form P–O–P and P–O–Ti linkages. As a result, most of the  $\text{OP}(\text{OEt})_3$  remains unreacted and is lost during heating.

The presence of carbon and hydrogen in the samples (see Table 1) is not unexpected for sol–gel derived materials. The C and some of the H is most likely present in the form of carbonised organic groups, whilst the remainder of the H is expected to be in hydroxyl groups. The presence of carbon and hydrogen has been accounted for by including C–C and P–OH correlations, at  $\sim 1.4$  and  $\sim 2.1$  Å, respectively, in the fitting of the diffraction data.

The measured densities for the two samples of  $\sim 2.4 \text{ g cm}^{-3}$  agree with each other within experimental error, suggesting an overall similarity between the two materials.

### 3.2. Neutron and X-ray diffraction measurements

Figs. 1 and 3, respectively, show the neutron and X-ray diffraction  $Q$ -space interference functions measured from the  $(\text{TiO}_2)_{0.5}(\text{P}_2\text{O}_5)_{0.5}$  sol–gel derived glasses. Figs. 2 and 4 show the pair distribution functions obtained by Fourier transformation of this data, together with the simulated analogues derived from the pair correlation fitting process described above. The structural parameters obtained from these simulations are given in Table 2. The errors in the figures given in Table 2 were estimated on the basis on how far a parameter could be varied without significantly

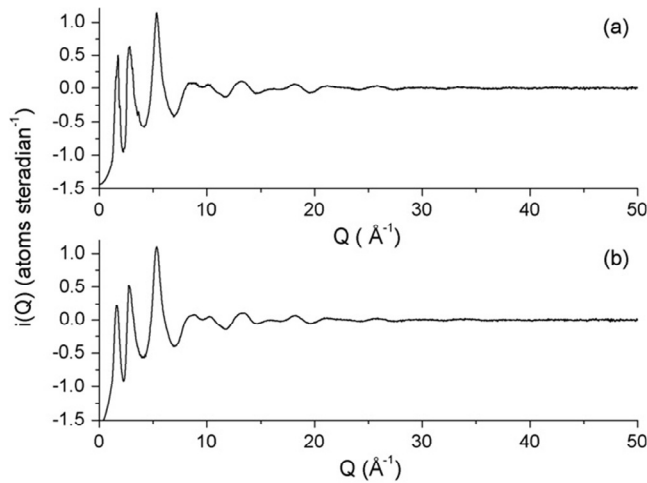


Fig. 1. Neutron diffraction  $Q$ -space interference functions,  $i(Q)$ , measured from the sol-gel derived  $(\text{TiO}_2)_{0.5}(\text{P}_2\text{O}_5)_{0.5}$  glasses: (a) P50T50A and (b) P50T50B.

changing the overall quality-of-fit, which was itself judged on the value of the discrepancy index,  $D$ , between the experimental data and the calculated simulation which is defined as:

$$D = \frac{\int |T^C(r) - T^E(r)| dr}{\int |T^E(r)| dr} \quad (5)$$

where the superscripts E and C refer to the experimental data and calculated simulation, respectively.

It is well known that the building blocks of phosphate-based glasses are  $\text{PO}_4^{3-}$  tetrahedra [11,12]. Each  $\text{PO}_4^{3-}$  can be connected to a maximum of three other such units to form a three-dimensional network, as in phosphorous pentoxide,  $\text{P}_2\text{O}_5$ . Metal oxides can be added to modify the network structure of the glass. Two P–O distances may be observed in phosphate glasses: a shorter distance of  $\sim 1.49 \text{ \AA}$  ascribed to bonds to non-bridging oxygens NBOs and a

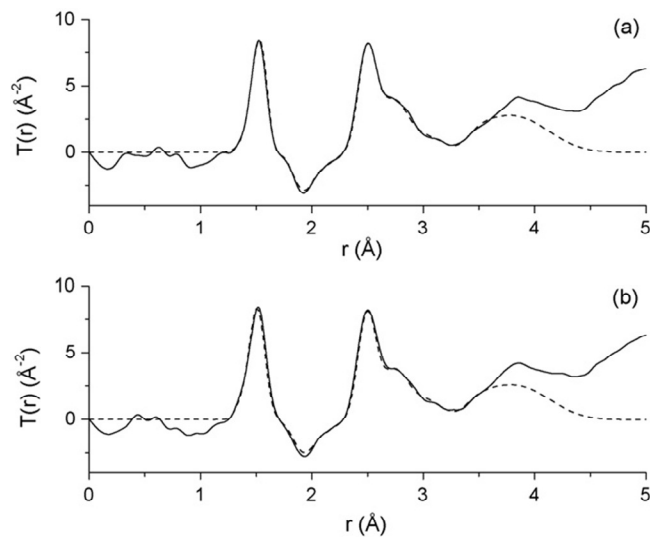


Fig. 2. Neutron diffraction pair distribution functions,  $T(r)$ , measured from the sol-gel derived  $(\text{TiO}_2)_{0.5}(\text{P}_2\text{O}_5)_{0.5}$  glasses (solid lines) together with the simulations obtained from the fitting process (dashed lines): (a) P50T50A and (b) P50T50B.

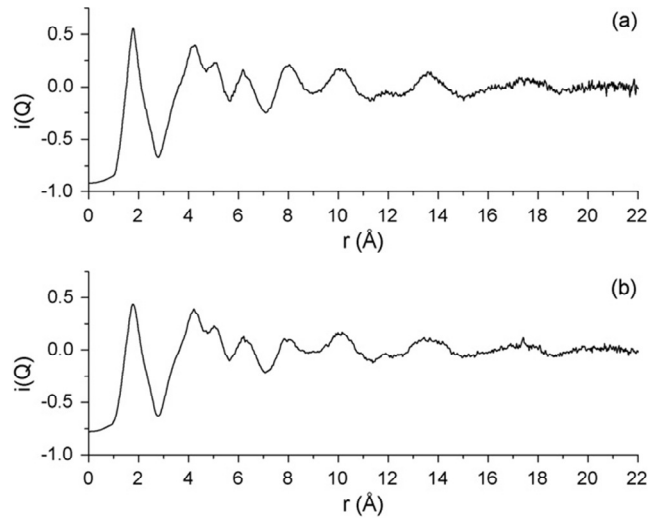


Fig. 3. X-ray diffraction  $Q$ -space interference functions,  $i(Q)$ , measured from the sol-gel derived  $(\text{TiO}_2)_{0.5}(\text{P}_2\text{O}_5)_{0.5}$  glasses: (a) P50T50A and (b) P50T50B.

longer distance of  $\sim 1.60$  Å due to bonds to bridging oxygens (BOs) [4,11,12]. The results in Table 2 indicate that such anticipated structural units are present in the sol-gel derived glasses studied here. Both samples show an average of  $\sim 4$  oxygens bonded to each phosphorus atom. Three of the four P–O bonds have a bond length of 1.50–1.51 Å, whilst the fourth has a bond distance of 1.57–1.58 Å; accordingly, these bonds are assigned to those to non-bridging and bridging oxygens, respectively.

Concerning the environment of titanium in these glasses, the results in Table 2 suggest that the  $\text{Ti}^{4+}$  ions are surrounded by 5.6–5.8 oxygens at a distance of 1.92–1.93 Å. The assignment of the peaks due to Ti–O bonding in the X-ray and neutron pair distribution functions is made easier by the negative neutron scattering length of titanium ( $b_{\text{Ti}} = -3.438$  fm, whereas  $b_{\text{O}} = 5.803$  fm). This means that the neutron weighting factor (see Eq. (3)) for the Ti–O correlation is negative, whereas the equivalent factor for X-rays is positive (the X-ray weighting factors roughly vary with the product of the atomic numbers of the elements concerned). The result is that the peaks due to Ti–O

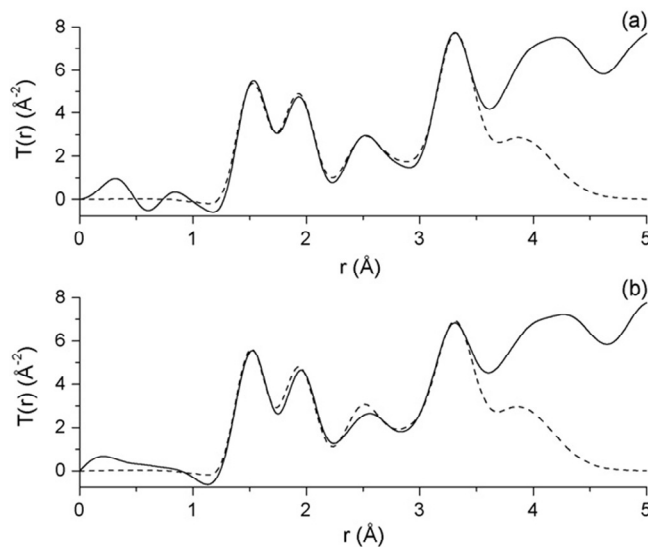


Fig. 4. X-ray diffraction pair distribution functions,  $T(r)$ , measured from the sol-gel derived  $(\text{TiO}_2)_{0.5}(\text{P}_2\text{O}_5)_{0.5}$  glasses (solid lines) together with the simulations obtained from the fitting process (dashed lines): (a) P50T50A and (b) P50T50B.

Table 2  
Structural parameters obtained from the simultaneous fitting of the neutron and HEXRD data

Sample	Correlation	$R$ (Å)	$N$	$\sigma$ (Å)
P50T50A	C–C	1.41(1)	1.7(2)	0.05(1)
	P–O	1.51(1)	2.9(1)	0.04(1)
	P–O	1.58(1)	1.1(1)	0.02(1)
	Ti–O	1.92(1)	5.6(2)	0.08(1)
	PO–H	2.11(2)	1.4(2)	0.09(2)
	O–O	2.50(1)	3.4(1)	0.07(1)
	O–O	2.73(2)	3.3(5)	0.13(2)
	P–P	3.00(3)	1.2(2)	0.09(4)
	P–Ti	3.31(2)	3.2(2)	0.10(2)
P50T50B	C–C	1.40(1)	2.0(2)	0.05(1)
	P–O	1.50(1)	2.9(1)	0.04(1)
	P–O	1.57(1)	1.0(1)	0.04(2)
	Ti–O	1.93(1)	5.8(2)	0.09(3)
	PO–H	2.12(2)	1.3(1)	0.09(1)
	O–O	2.49(1)	3.7(5)	0.07(1)
	O–O	2.74(2)	3.4(4)	0.13(2)
	P–P	3.00(1)	1.7(3)	0.08(3)
	P–Ti	3.31(1)	2.65(2)	0.10(2)

correlations appear negative-going in the neutron pair distribution function and positive-going in the equivalent X-ray function. Titanium–oxygen bond distances exhibit a strong correlation with coordination number: average Ti–O bond distances for 4-coordinated Ti fall in the range 1.71–1.83 Å, whereas those for 5-coordinated Ti range from 1.88 to 1.92 Å and those for 6-coordinated Ti range from 1.92 to 2.04 Å. The average Ti–O bond distance and coordination number measured here lend themselves to the conclusion that titanium occupies an octahedral site in the phosphate glass, although these parameters are not inconsistent with a mixture of five- and six-fold coordination with a predominance of the latter.

The O–O distances measured give information on the PO<sub>4</sub> and TiO<sub>6</sub> polyhedra that comprise the glass structure. Taking an average P–O bond length of 1.52 Å and assuming a tetrahedral angle of 109°, the calculated average O–O distance for the PO<sub>4</sub> group is 2.49 Å which agrees well with the shorter measured O–O distance of 2.49–2.50 Å. Following a similar process for a TiO<sub>6</sub> octahedron with an average Ti–O bond length of 1.93 Å, we arrive at an O–O distance of 2.73 Å which agrees with the longer measured O–O distance. Again, this result does not categorically rule out the presence of some 5-coordinated Ti. Trigonal bipyramidal five-fold Ti would have an average O–O distance of 2.93 Å, whereas a square pyramidal arrangement of oxygens would have an average O–O distance close to that of the TiO<sub>6</sub> octahedron (probably slightly greater due to the electrostatic repulsion of the oxygens). However, the identification of an O–O distance of 2.73 Å is at least consistent with the majority of the titanium occupying an octahedral site.

The remaining parameters in Table 2 yield information on how the PO<sub>4</sub> and TiO<sub>6</sub> polyhedra are connected together to form the glass network. A peak at ~3 Å is required to obtain a satisfactory fit to the scattering data from both samples. The position of this peak agrees well with the P–P nearest neighbour distance measured in other phosphate glasses [12] and results from corner sharing PO<sub>4</sub> tetrahedra with a P–O–P bond angle of 121°. The feature at 3.31 Å in the pair distribution functions is assigned to the P–Ti nearest neighbour distance. The accurate assignment and fitting of this feature again benefits from the negative neutron scattering length of Ti which results in a negative peak in the neutron pair distribution function and a positive one in the equivalent X-ray function. Without both sets of complementary neutron and X-ray data, it would be difficult to fit the P–Ti correlation with any degree of certainty. The distance of 3.31 Å for the P–Ti correlation is in the range expected for corner sharing PO<sub>4</sub> and TiO<sub>6</sub> polyhedra. The coordination numbers associated with the P–P and P–Ti correlations of 1.2–1.7 and 2.7–3.2, respectively, suggest that on average each PO<sub>4</sub> tetrahedron shares one bridging oxygen with another PO<sub>4</sub> group and three non-bridging oxygens with TiO<sub>6</sub> octahedra. The P–P coordination number obtained for the P50T50B sample is a little high, even considering the larger errors associated with fitting overlapping correlations in pair distribution functions. Despite this, the proposed arrangement of PO<sub>4</sub> and TiO<sub>6</sub> polyhedra is consistent with the ratio of bridging to non-bridging oxygens of 1:3 determined by the fitting of the P–O correlation.

In order to obtain a satisfactory fit to both the neutron and X-ray pair distribution functions, it was necessary to include a P–H correlation at  $\sim 2.1$  Å. This correlation contributes negative intensity to the neutron  $T(r)$  because of the negative scattering length of hydrogen ( $b_{\text{H}} = -3.739$  fm) and very little intensity to the X-ray  $T(r)$  due to the low atomic number of hydrogen. The phosphorus–hydrogen distances in Table 2 of 2.11–2.12 Å are very close to that found in the P–OH groups in  $\text{H}_3\text{PO}_4$  [13]. Thus, the ND data provides evidence of the presence of P–OH groups in the glass structure. This is perhaps not surprising given that the elemental analysis shows the presence of hydrogen in the samples and that sol–gel glasses in general have network structures that are not fully connected, with OH groups usually terminating and charge balancing the associated non-bridging oxygens.

The structural parameters obtained for the C–C correlation are consistent with the presence of hydrogenated carbon. The C–C distance measured here of 1.40–1.41 Å is in close agreement with that of 1.42 Å found in graphite [10] and that of 1.40 Å found in benzene [14]. Hence, the measured bond distance suggests that the carbon is  $\text{sp}^2$  hybridised. The C–C coordination numbers are a little lower than the expected value of 3 for a graphite-like structure, suggesting that there are significant C–H bonds present.

Inspection of the structural parameters in Table 2 reveals that, if the estimates of the errors are taken into consideration, there are no significant atomic-scale structural differences between the sample prepared by the acid-catalysed reaction and that prepared by the base-catalysed reaction.

### 3.3. Reverse Monte Carlo Modelling

When trying to understand the structure of glasses, it is often useful to look at the structure of closely analogous crystalline compounds. In this case, the compound  $\text{TiP}_2\text{O}_7$  is very close in composition to the glasses prepared here. The structure of  $\text{TiP}_2\text{O}_7$  consists of  $\text{TiO}_6$  octahedra and  $\text{PO}_4$  tetrahedra sharing corners in a three-dimensional network [9]. The  $\text{PO}_4$  tetrahedra form  $\text{P}_2\text{O}_7$  groups connecting the  $\text{TiO}_6$  octahedra. The similarity between the features of the glass structure described in the previous paragraphs and the structure of  $\text{TiP}_2\text{O}_7$  is immediately obvious: in essence, both structures share the same building blocks. Table 3 includes the structural parameters that define the short- to medium-range order in the structure of  $\text{TiP}_2\text{O}_7$ . There is excellent agreement between the bond distances in  $\text{TiP}_2\text{O}_7$  and those measured from the sol–gel derived  $(\text{TiO}_2)_{0.5}(\text{P}_2\text{O}_5)_{0.5}$  glasses given in Table 2, suggesting that the short and intermediate range order in the two structures is very similar. In order to further elucidate the similarity in structure between  $\text{TiP}_2\text{O}_7$  and  $(\text{TiO}_2)_{0.5}(\text{P}_2\text{O}_5)_{0.5}$  glass, the superstructure of  $\text{TiP}_2\text{O}_7$  was used as the starting configuration in RMC modelling of the X-ray data from the glass. Fig. 5 shows a comparison of the  $i(Q)$  from the RMC model with that from the P50T50A sample. The agreement between the two curves is good and the discrepancies are well within the possible errors in the experimental data that result from the data reduction and correction processes. Thus, Fig. 5 illustrates that a model consisting of corner-sharing  $\text{PO}_4$  tetrahedra and  $\text{TiO}_6$  octahedra can indeed provide a satisfactory quantitative fit to the experimental data. Interrogation of the RMC model yields the structural parameters in Table 3. The structural parameters from the model serve to reinforce the close relationship between the near-neighbour structure of  $\text{TiP}_2\text{O}_7$  and that of a glass of comparable composition. However, there are important differences. Both the O–O and P–Ti coordination numbers are lower in the RMC model. This is indicative of less connectivity between the  $\text{PO}_4$  and  $\text{TiO}_6$  polyhedra in the final model compared to

Table 3  
Structural parameters for crystalline  $\text{TiP}_2\text{O}_7$  and those obtained from the RMC model of the P50T50A glass sample

Correlation	$\text{TiP}_2\text{O}_7^a$		RMC model	
	$R$ (Å)	Total $N$	$R$ (Å)	Total $N$
P–O	1.52	4	1.52	4.0
Ti–O	1.92	6	1.93	6.0
O–O	2.50	7	2.52	6.6
	2.70		2.80	
P–P	3.01	1	3.07	1.0
P–Ti	3.30	3	3.29	2.8

<sup>a</sup> Taken from ref. [10].

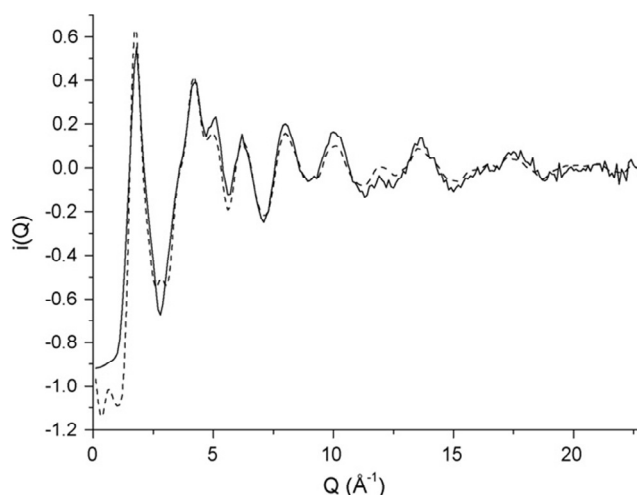


Fig. 5. RMC fit (dashed line) to the HEXRD  $i(Q)$  function (solid line) measured from the P50T50A sample.

the crystalline starting configuration. As mentioned earlier, this result is not unexpected considering we are modelling data derived from a sol–gel glass and supports the assignment of a correlation due to P–OH groups in the ND data.

It should be stressed that the RMC derived model obtained is not a unique solution to puzzle of finding a three-dimensional arrangement of atoms consistent with experimental data; however, despite this limitation, it provides a useful aid to the interpretation of the ND and HEXRD data.

#### 4. Conclusions

A method for the sol–gel synthesis of binary  $(\text{TiO}_2)_{0.5}(\text{P}_2\text{O}_5)_{0.5}$  glasses has been developed that can be employed to prepare samples using either an acidic or basic catalyst. Relatively low phosphorous losses were observed upon drying and heat treatment, suggesting good chemical bonding between the two oxide components in the gel state. Analysis of the neutron and X-ray diffraction data revealed that the structure of the heat-treated glass consists of corner sharing  $\text{TiO}_6$  octahedra and  $\text{PO}_4$  tetrahedra with the latter present as  $\text{P}_2\text{O}_7$  groups connecting the  $\text{TiO}_6$  octahedra. The presence of a minority  $\text{TiO}_5$  component cannot be completely excluded. The Reverse Monte Carlo method was used to produce a structural model and to illustrate that the structure of the glass is very similar to the superstructure of crystalline  $\text{TiP}_2\text{O}_7$  at the near-neighbour level. Whereas the structure of  $\text{TiP}_2\text{O}_7$  consists of a fully connected network, the proposed network structure of the glass has some of the non-bridging oxygen atoms terminated by protons. Evidence for this comes from the observation of a correlation due to P–OH bonding in the ND data and from the lower than anticipated (for a fully consolidated network) O–O and P–Ti coordination numbers derived from the model. The presence of OH groups is important because these play a role in the protonic conductivity of such materials [15]. No significant structural differences were observed between glasses prepared by acid- or base-catalysed sol–gel reactions at the atomic level, although there may be differences in the textural structure, such as pore size and pore connectivity.

By combining the complimentary techniques of ND and HEXRD, we have directly observed the atomic-scale correlations. The combination of techniques allows accurate assignment of these correlations and reduces the errors associated with the bond distances and coordination numbers obtained. Therefore, aside from providing a characterisation of the structure of  $(\text{TiO}_2)_{0.5}(\text{P}_2\text{O}_5)_{0.5}$  sol–gel derived glasses, this work illustrates the benefit of combining neutrons and X-rays when studying amorphous materials; either technique alone could not provide such detailed and accurate structural information.

#### Acknowledgements

The authors wish to acknowledge funding from the EPSRC (EP/C000714, EP/C000633 and GR/T21080) and the use of the EPSRC's Chemical Database Service at Daresbury. We thank A.C. Hannon of the CCLRC Rutherford

Appleton Laboratory for his help in running GEM, and A. Lennie of the CCLRC Daresbury Laboratory for his assistance in the use of Station 9.1.

## References

- [1] K. Makita, M. Nogami, Y. Abe, *J. Mater. Sci. Lett.* 16 (1997) 550.
- [2] H. Nasu, K. Kamiya, *Mater. Res. Bull.* 40 (2005) 55.
- [3] T. Kasuga, M. Nogami, M. Niinomi, *Mater. Sci. Forum* 426 (2003) 3183.
- [4] A.C. Hannon, *Nucl. Instrum. Methods A* 551 (2005) 88.
- [5] B.E. Warren, *X-ray Diffraction*, Dover, New York, 1990.
- [6] J.M. Cole, E.R.H. van Eck, G. Mountjoy, R. Anderson, T. Brennan, G. Bushnell-Wye, R.J. Newport, G.A. Saunders, *J. Phys. Condens. Matter* 13 (2001) 4105.
- [7] P.H. Gaskell, in: J. Zrzycky (Ed.), *Materials Science and Technology*, vol. 9, VCH, Weinheim, 1991, p. 175.
- [8] R.L. McGreevy, P. Zetterström, *J. Non-Cryst. Solids* 293-295 (2001) 297.
- [9] S.T. Norberg, G. Svensson, J. Albertsson, *Acta Crystallogr., Sect. C: Cryst. Struct. Commun.* C57 (2001) 225.
- [10] D.A. Fletcher, R.F. McMeeking, D. Parkin, The United Kingdom Chemical Database Service, *J. Chem. Inf. Comput. Sci.* 36 (1996) 746.
- [11] R.K. Brow, *J. Non-Cryst. Solids* 263-264 (2000) 1.
- [12] U. Hoppe, G. Walter, R. Kranold, D. Stachel, *J. Non-Cryst. Solids* 263-264 (2000) 29.
- [13] M. Souhassou, E. Espinosa, C. Lecomte, R.H. Blessing, *Acta Crystallogr., Sect. B: Struct. Sci.* B51 (1995) 661.
- [14] L.E. Sutton, *Tables of Interatomic Distances and Configurations in Molecules and Ions* (Special Publication No. 18), The Chemical Society, London, 1965.
- [15] G. Li, M. Nogami, Y. Abe, *Solid State Ionics* 83 (1996) 209.